


EOSAM 2022

Guest editors: Patricia Segonds, Gilles Pauliat and Emiliano Descrovi

RESEARCH ARTICLE

OPEN ACCESS

Digital speckle photography in the presence of displacement gradients

León Schweickhardt* , Andreas Tausendfreund, Dirk Stöbener, and Andreas Fischer

University of Bremen, Bremen Institute for Metrology, Automation and Quality Science, Linzer Str. 13, 28359 Bremen, Germany

Received 19 January 2023 / Accepted 20 March 2023

Abstract. Digital speckle photography is a displacement field measurement method that employs laser speckles as surface markers. Since the approach requires only one reference image without a preparation of the sample and provides a fast, single-shot measurement with interferometric precision, the method is applied for in-process measurements in manufacturing engineering. Due to highly localized loads, higher-order displacement gradients occur in manufacturing processes and it is an open research question how these gradients affect the measurement errors of digital speckle photography. We simulate isotropic Gaussian surface topographies, apply a displacement field and then generate laser speckle patterns, which are evaluated with digital image correlation and subsequently the resulting random and systematic errors of the displacement field are analyzed. We found that the random error is proportional to the first-order displacement gradient and results from decorrelation of the laser speckles. The systematic error is mainly caused by the evaluation algorithm and is linearly dependent on the second-order gradient and the subset size. We evaluated in-process displacement measurements of laser hardening, grinding and single-tooth milling where we determined the relative error caused by displacement gradients to be below 2.5% based on the findings from the simulative study.

Keywords: Digital speckle photography, Digital image correlation, Displacement gradients, Systematic errors.

1 Introduction

Surface layer properties such as residual stresses and hardness determine the service life and performance of a workpiece [1]. In order to achieve the desired surface parameters a measurement of material stresses during the manufacturing process is required [2]. Digital image correlation (DIC) is a fast non-contacting method for the in-process measurement of displacement fields from a pattern of random, previously applied markers on the surface. Digital speckle photography (DSP) uses the same image correlation method and employs laser speckles as optical surface markers for a non-invasive measurement without the need to prepare the sample surface. However, considering cutting manufacturing processes such as milling, turning and grinding, the load of the material is heavily localized and, thus, displacement gradients occur. As of yet, a study on the impact of displacement gradients on DSP, considering both the random and systematic error, is missing.

Through the rapid development of digital image sensors and image processing, DIC has become an established

technique for the measurement of surface displacement fields [3]. The measurement setup for in-plane displacement fields is simple and flexible as it requires only a digital camera and can thus be applied in various fields from nanoscale displacement measurements on biological materials [4] to the aerial drone-based inspection of the structural health of bridges [5]. In principal, sequential image pairs of the surface are divided into subsets and for each subset-pair the local displacement components are calculated by image tracking algorithms that are either based on cross-correlation or least-squares approaches [6]. For measurement objects with discontinuous deformation fields, as in the case of crack formation, there are also algorithms for pointwise digital image correlation that are able to determine a local displacement value at each pixel [7]. The surface displacement is tracked through white light speckle patterns that are artificially applied – for instance with paint, spin coating or lithography [8] – or laser speckle patterns. The distinction is fundamentally important, as white light speckles are physically applied to the surface and follow all its displacements. Laser speckles, however, are an interference phenomenon caused by the scattering of coherent illumination on rough surfaces. Therefore, no preparation of the sample surface is required for DSP, but a laser is

* Corresponding author: l.schweickhardt@bimaq.de

necessary in the experimental setup and decorrelation of the speckle patterns can occur for an excessive rigid body motion or out-of-plane displacement [9].

DSP is a non-invasive measurement technique for displacement fields on planar surfaces. The measurand is an in-plane displacement and the optical axis of the camera should be aligned to be perpendicular to the sample surface. While this study focuses on measuring in-plane displacement with a single-camera setup, the measurement setup can be expanded to also detect out-of-plane displacement, for instance by means of speckle decorrelation [10, 11] or by integrating a stereomicroscope [12] or shearography [13]. With DSP, rigid-body displacements can be measured with single-digit nanometer resolution, while the achievable measurement uncertainty with fully developed speckle is only limited by Heisenberg's uncertainty principle, if a large number of speckles is evaluated to minimize the speckle noise [14, 15]. An enhanced study in [16] describes the achievable random measurement error for a non-negligible speckle noise, i.e. the fixed pattern noise resulting from a small number of speckle in the subset <100 , and camera noise in addition to the photon shot noise. Note that the statistical properties of the laser speckle field can be customized with a phase-only spatial light modulator (SLM) [17]. In particular, an SLM allows the generation of multiple uncorrelated speckle patterns and thus a reduction of the random error by an order of magnitude through ensemble averaging [15]. DSP was applied in various manufacturing processes and material tests: In hole drilling to measure residual stress [18], in high temperature tensile tests [19], during single-tooth milling [20], grinding [21], electro-hydraulic extrusion [16] and deep rolling [11]. In these practical applications higher-order displacement gradients generally occur due to localized loads, inhomogeneous material properties, holes, or notches. While it was reported that displacement gradients increase the decorrelation in DSP [22], the extent of the resulting random and systematic errors for these applications still remains unknown.

Displacement gradients were theoretically shown to cause systematic errors that are proportional to the second-order displacement gradient in DIC with white light speckles [23]. In certain applications such as the measurement of local deformations near crack tips during material testing [24] exceptionally high local displacement gradients occur. Using high-speed photography with 200,000 frames per second, displacement fields were measured during crack propagation, which resulted in local first-order gradients of around $2000 \mu\epsilon$ concentrated around the crack tip [25]. These gradients were shown to cause significant systematic errors $> 1 \mu\text{m}$, which equated to 10% of the DIC subset width or 5% of the total displacement amount [23]. Thus, the following questions yet remain unanswered regarding DSP in the presence of displacement gradients:

1. How is the random error affected?
2. What systematic errors occur?
3. Do displacement gradients significantly impact the measurement uncertainty budget of DSP in in-process applications such as milling, grinding or laser hardening?

The principal aim of this article is to present and apply a DSP simulation setup to predict the random and systematic errors caused by displacement field gradients. Additionally, DSP measurements from multiple in-process manufacturing applications are evaluated in order to estimate the measurement errors resulting from displacement gradients. The DSP measurement principle is explained in Section 2 and the simulation setup of the measurement chain is shown in Section 3. In the subsequent results Section 4, the simulated behavior of the random and systematic errors in dependence of the measurement parameters is presented first. Based on these data sets a heuristic model is developed in order to correct systematic errors due to displacement gradients. Finally, results from DSP measurements of workpiece surfaces during different manufacturing processes are presented and the correction model is applied to the experimental data. Section 5 concludes the article and gives an outlook on further research aspects.

2 Measurement principle

Laser speckles occur when a surface that is rough on the scale of the wavelength is illuminated with a coherent light source. The height differences of the surface topography cause local phase variations of the scattered light and, thus, lead to constructive or destructive interference in the image plane. In this study, we consider subjective speckle patterns, i.e. the interference pattern is observed through an imaging system. Therefore, the size of the speckles in the image plane can be adjusted by varying the aperture. As each speckle is formed by the scattering from certain nanoscale surface structures, a lateral rigid-body displacement of the surface causes a displacement of the observed speckle pattern that can be tracked through DIC. However, when deformation occurs, the lateral structure of the surface changes, which affects the speckle pattern. It is important to note that the laser speckles do not experience the same deformation as the underlying surface elements. The shape and size of a speckle can change locally, but a surface deformation can also lead to new speckles appearing or disappearing [9]. These local changes in the speckle pattern cause a decorrelation of the corresponding image subsets when the displacement field is calculated with a DIC algorithm.

The task of the DIC algorithm is to find the local displacement values of each subset. Figure 1 shows a section of a speckle pattern with the grayscale values $f(\mathbf{X})$ before and $g(\mathbf{y}(\mathbf{X}))$ after deformation. The exemplary subset (red square) experiences the displacement and deformation $\mathbf{y}(\mathbf{X})$. The inverse problem of the measurement is to find the $\mathbf{y}(\mathbf{X})$ that satisfies the condition $f(\mathbf{X}) = g(\mathbf{y}(\mathbf{X}))$ best. However, equality can only be achieved in the ideal, theoretic case, where the grayscale values do not change from the deformation. During actual measurements in the presence of random noise and other sources of error, solving the inverse problem leads to an optimization task, which can be stated as the squared differences of the grayscale values [6]:

$$C = \int |f(\mathbf{X}) - g(\mathbf{y}(\mathbf{X}))|^2 d\mathbf{X} \rightarrow \text{minimize over } \mathbf{y}. \quad (1)$$

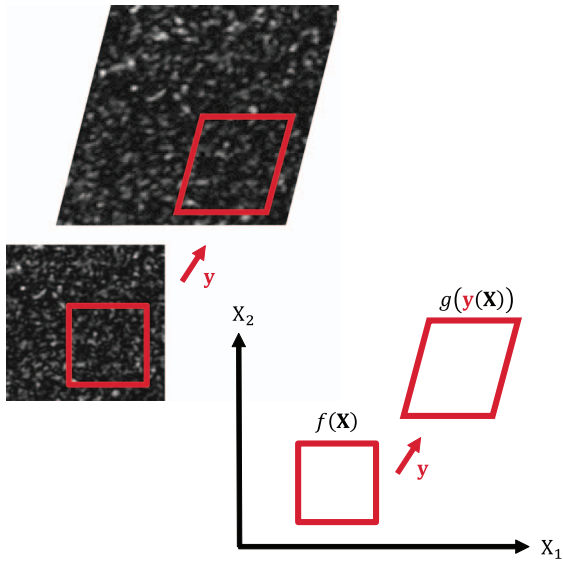


Figure 1. Section of a speckle pattern before (square) and after (parallelogram) the deformation $\mathbf{y}(\mathbf{X})$. The red squares represent exemplary subsets with the grayscale values $f(\mathbf{X})$ and $g(\mathbf{y}(\mathbf{X}))$.

Another common approach is to calculate the cross-correlation of $f(\mathbf{X})$ and $g(\mathbf{y}(\mathbf{X}))$ in order to find $\mathbf{y}(\mathbf{X})$ [16, 26]. Displacement gradients pose two main challenges to both the least-squares and cross-correlation image processing approaches:

- Undermatched or overmatched shape functions
- Decorrelation between f and g (only for laser speckles)

The first stems from the practical implementation of the DIC algorithm. In order to find its local displacement values, the subset $f(\mathbf{X})$ is displaced stepwise and may also be deformed through certain shape functions until it most closely matches $g(\mathbf{y}(\mathbf{X}))$, i.e., until C in equation (1) is minimized. Modern DIC algorithms often include the shape functions for rotation, shear, first-order gradients, and second-order gradients [27, 28]. When the measured displacement gradients are of a higher order than the shape function it is undermatched and when the shape function is of a higher order than the measurand it is overmatched. Undermatched shape functions are known to cause systematic errors in DIC. However, overmatched shape functions were found to cause measurement error as well [29]. Therefore, the DIC algorithm should be adjusted to the measurand, whenever possible. In Section 4.3, we evaluate three experimental studies, where the shape function is undermatched and estimate the resulting random and systematic errors. The second source of error affects only DSP, because laser speckle patterns inherently change under displacement gradients. While undermatched shape functions cause systematic errors in DIC, decorrelation of laser speckles is a cause for random errors in the DSP displacement measurement [22].

3 Simulation setup

In order to statistically study the effect of different displacement gradients on DSP and quantify the resulting errors, the measurement object and measurement system are simulated in MATLAB. The simulation setup is schematically shown in Figure 2. The measurement object is an isotropic, Gaussian surface with the roughness $S_q = 0.07 \mu\text{m}$ and a lateral correlation length $L = 20 \mu\text{m}$. The surface topography is simulated according to the moving average method [30]. In order to more accurately represent subpixel displacements and avoid aliasing during the downsampling process, the surface is simulated with a resolution 30 times higher than the final speckle pattern. The upsampling factor of 30 was found to be sufficiently high, so that constant subpixel displacements could be evaluated without significant systematic errors. Here, for a speckle pattern of 256 by 256 pixels with a pixel size of $3.45 \mu\text{m}$, a surface topography of 7680 by 7680 pixels with a pixel size of $0.115 \mu\text{m}$ is simulated. Subsequently, a displacement field is applied to the surface with the `imwarp()` function.

Speckle patterns for both surface topographies are then simulated according to Goodman, sample code can be found in appendix G2 of [9]. In place of his variable *randomfield*, an $n \times n$ matrix of random phasors, we use the original and deformed simulated surface topographies. The inclusion of the surface simulation by means of the moving average method allows an adjustment of the roughness and correlation length of the isotropic surface topography and, thus, represents an expansion of Goodman's simulation algorithm. To perform the simulation, the size of the matrix of the surface must be equal to the size of the matrix of the speckle pattern. Therefore, the original and deformed surface are downsampled by a factor of 30. The influence of the bicubic interpolation was studied by evaluating the deformed surface topographies with and without interpolation using DIC, and it was found to be negligible. The simulated speckle pattern is fully polarized, fully developed, with a wavelength of 638 nm. The aperture D of the optical system is adjusted to obtain a speckle size of 3 pixels, i.e. $10.35 \mu\text{m}$ for the pixel size of $3.45 \mu\text{m}$. Several authors have reported that speckle sizes of 2–5 pixels minimize the random error [20, 31]. An augmented-Lagrangian digital image correlation algorithm [6] that uses equation (1) is used to calculate the resulting displacement fields. This algorithm combines the speed of local subset DIC and the kinematic compatibility of global DIC. While local subset DIC does allow for faster computation, the results can be noisy and lead to discontinuous strain fields. The augmented-Lagrangian DIC algorithm uses local subsets with the added global constraint of a continuous first-order displacement gradient. Finally, the DIC result is compared to the predefined displacement field. The true values of the displacement field vary only along the abscissa. Thus, the mean along the ordinate axis is calculated for the error field. The deviation of the mean from the respective true value yields the systematic error, while the standard deviation of the mean along the ordinate yields the random error.

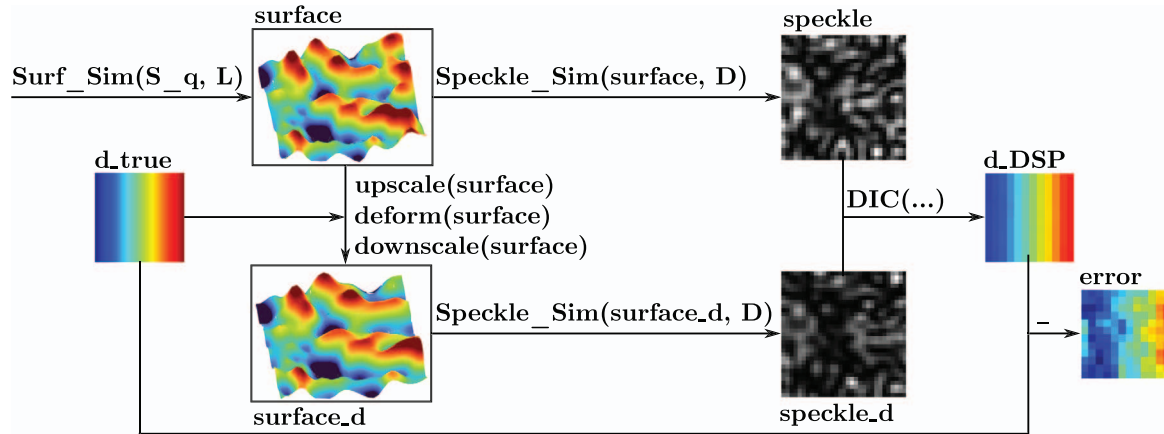


Figure 2. Speckle simulation setup.

4 Results

4.1 Random error

The random error caused by displacement gradients is investigated with the simulation setup described in Section 3. For this purpose a displacement field is chosen, which allows the study of the effects of first- and second-order displacement gradients. Higher-order gradients are not considered, as they did not occur in our experimental studies [20, 21, 32]. The displacement field consists of the following four sections along the x -axis:

- (I) A constant displacement of 1 pixel.
- (II) A constant positive second-order displacement gradient.
- (III) A constant negative second-order gradient whose absolute value is equal to that of section II.
- (IV) A constant displacement of d_{max} .

An example of the resulting displacement derivative over x , i.e., the first-order gradient in x -direction, with the four sections is shown in Figure 3a, red curve. In addition to the parameter d_{max} , the length of the interval x_{int} of sections II and III is subsequently varied in order to study the effect of different displacement gradients. For the example shown in Figures 3a and 3b, $d_{\text{max}} = 6$ pixels and $x_{\text{int}} = 100$ pixels. Along the y -axis the true value of the displacement field is always constant.

Figure 3b shows a part of the displacement field that is measured on the basis of the deformed surface and the simulated speckle patterns (corresponds to d_{DSP} in Fig. 2). The subset size of the DIC algorithm is 20×20 pixels and the step size is 1 pixel, i.e., the subset is moved in 1 pixel increments over the speckle pattern resulting in local displacement values $d_x(x, y)$ and $d_y(x, y)$ at every pixel of the original speckle pattern except on the edges. Due to random errors, the local displacement d_x varies visibly along the y -axis. One displacement field and speckle pattern is 256 by 256 pixels wide, but for each displacement parameter set, 50 unique surface topographies of the same statistic parameters and speckle patterns are generated in order to

increase the sample size. The random error is quantified by the standard deviation along the y -axis over all samples. In Figure 3a, the solid lines show the random error calculated from the displacement field d_x of Figure 3b in blue together with the true value of the displacement gradient in red. The dashed lines show an alternative displacement field with a constant first-order gradient of $10 \times 10^4 \mu\text{e}$ in sections III and IV. The random error of the alternative displacement field remains constant in sections III and IV, even though the absolute value of the displacement increases, thereby demonstrating that the random error is only dependent on the first-order gradient of the displacement. The gradient is scaled in, i.e., in displacements d_x of 10^{-6} pixels over a length of 1 pixel in x -direction. In Sections I and IV of constant displacement values, the random error is nearly constant in x -direction at around 0.02 pixels. Note that the random error does not change with the absolute displacement value, which is 1 pixel in section I and 6 pixels in section IV. In both sections the random error is mainly dependent on the subset size, with a larger subset decreasing the random error. This decrease is due to a higher number of speckles being evaluated in a larger subset [16]. The speckle size is 3 pixels, which lies in the optimal range of 2–5 pixels that is generally reported for DSP [31]. For speckle sizes < 2 pixels or > 5 pixels, the random error increases significantly. In this study, random errors caused by camera noise, shot noise or other external factors are not considered. Thus, the observed random error is inherent to the DIC evaluation and the laser speckle patterns.

The relation between the displacement gradient and the random error is further investigated in Figure 4. Here, the maximum random error, which occurs close to the point of the highest displacement gradient, is plotted over the varied gradient. For each gradient value, the subset sizes 10, 14 and 20 pixels are analyzed. In addition to the DSP results, the random error of a DIC evaluation of the surface topography is shown. For the latter case, the simulation of the speckle patterns (“`Speckle_Sim()`” in Fig. 2) is omitted. The DSP results show a correlation between random error and displacement gradient on the one hand and the random error and subset size on the other hand. Moreover, the comparison of DSP and DIC without laser speckles indi-

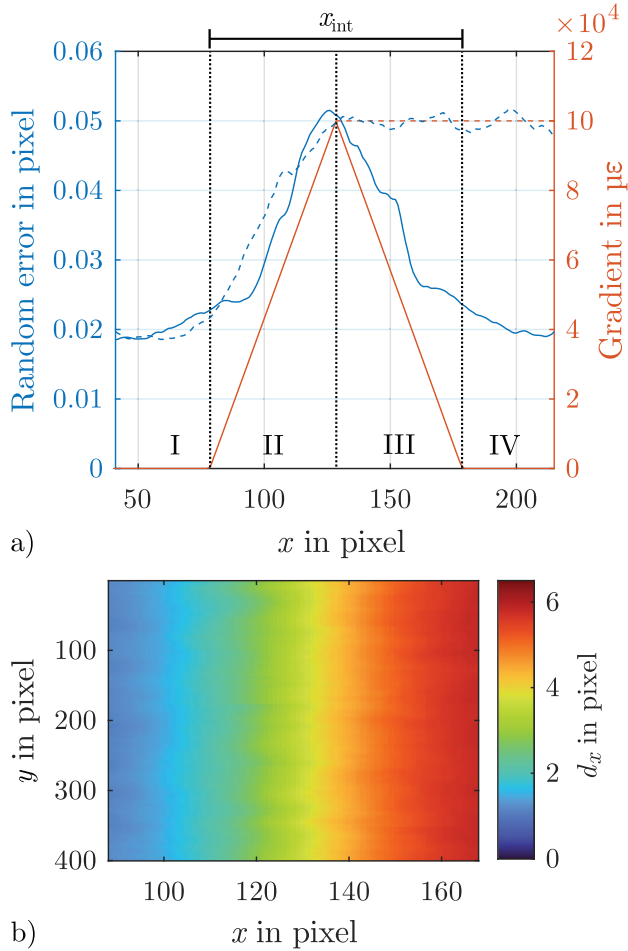


Figure 3. (a) True value of the displacement gradient in x -direction (red) and random error of d_x (blue), i. e., the standard deviation of d_x in y -direction. Dotted vertical lines indicate the four numbered sections of the displacement field. Sections I and IV are characterized by a constant displacement value, while sections II and III have a constant second-order displacement gradient. Subset size $S = 20 \times 20$ pixel. The dashed lines show an alternative displacement field with a constant first-order gradient of $10 \times 10^4 \mu\text{e}$ in sections III and IV. (b) DSP result d_x in x -direction. The displacement field is evaluated from simulated speckle patterns.

icates that the observed DSP errors are in fact predominantly due to the properties of the laser speckle patterns in the presence of displacement gradients and not due to the DIC evaluation. The DIC results also demonstrate a small linear increase of the random error from 1.5×10^{-3} pixels to 3×10^{-3} pixels. However, in the presence of displacement gradients these values are negligible compared to the random errors of DSP. Note that evaluating the surface topography matrix directly with the DIC algorithm is naturally not a realistic use case. This comparison was chosen in order to prove that the random errors in the presence of displacement gradients are not due to the DIC algorithm, but due to the laser speckle pattern. Laser speckles do not deform in the same way the underlying surface topography does and, thus, decorrelation occurs. This decorrelation be-

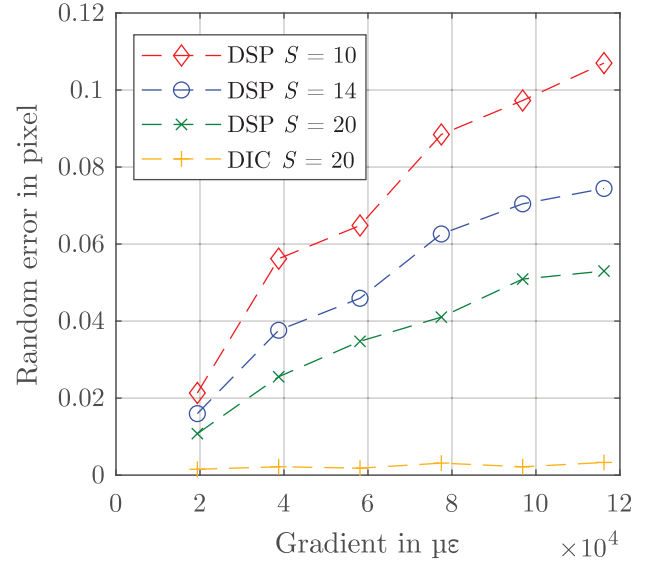


Figure 4. Random error of displacement field d_x for three different subset sizes S . The random error is evaluated from laser speckle patterns (DSP) and evaluated directly from the deformed surface topography (DIC).

tween the original and the deformed laser speckle pattern is the cause for the increasing random error of the DSP results shown in Figure 4 and the disparity between the DSP and DIC results.

4.2 Systematic error

In order to obtain the systematic error, first the random error must be eliminated from the displacement results through averaging over a large sample size. For this purpose, multiple surface topographies and respective speckle patterns are simulated as in Section 4.1. The arithmetic mean in y -direction of the two-dimensional displacement field $d_x(x, y)$ then yields $\bar{d}_x(x)$ with the random error minimized. Figure 5a shows the mean displacements in x -direction $\bar{d}_x(x)$ of the DSP result compared to the true value and a moving mean of the true value over 20 pixels in x -direction. The difference of the mean displacement \bar{d}_x and the true value is the systematic error of the DSP measurement. In Figure 5a the systematic error can be seen qualitatively as the deviation of the red and blue dots from the green line that represents the true value. Evidently, systematic errors also occur for the moving mean in the presence of higher-order displacement gradients. The mathematical reason for the resulting errors is that for a nonlinear $\bar{d}_x(x)$, the mean value of an interval is not equal to the value at the center of the interval. However, the systematic errors of the DSP results are significantly higher than those of the moving mean and, thus, cannot be explained solely by spatial averaging over the subset.

For a quantitative analysis, the the systematic error is plotted in Figure 5b and is compared with the Laplacian, i.e., the second-order gradient. In theory, the Laplacian is zero in sections I and IV (see Fig. 3a for a visual representation of these sections) and has the same constant, positive

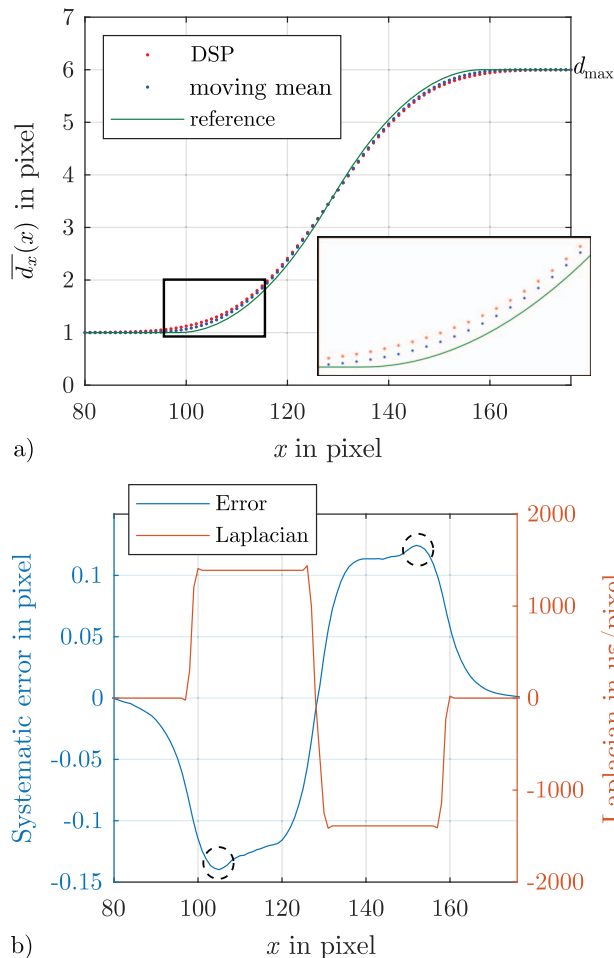


Figure 5. (a) Mean in y -direction of the displacement field $d_x(x, y)$ yields $\bar{d}_x(x)$. The DSP result ($S = 20$ pixels) is compared to its true value and a moving mean of the true value over 20 pixels in x -direction. (b) Laplacian of the displacement d_x and systematic error over x . The systematic error is the deviation of \bar{d}_x from the true value.

or negative value in sections II and III, respectively. Note that in Figure 5b the Laplacian calculated with MATLAB is shown, which is why deviations from the theory occur at the theoretical discontinuities between the sections. The systematic error shows similar characteristics as the Laplacian: In the presence of the Laplacian the systematic error increases abruptly and is relatively constant for a constant Laplacian. The symmetric maxima that are indicated in Figure 5b with dashed circles at the beginning of section II and the end of section III indicate the a sensitivity of the systematic error to the change of the Laplacian, i.e., to the third-order gradient. The smoother course of the systematic error in comparison to the discontinuous Laplacian can be explained on the one hand by the spatial averaging of the subsets and on the other hand by the global approach of the DIC algorithm that was introduced in Section 2. The aim of the global approach is to find a continuous displacement field that most closely matches the local displacement values calculated in the subsets. This approach generally

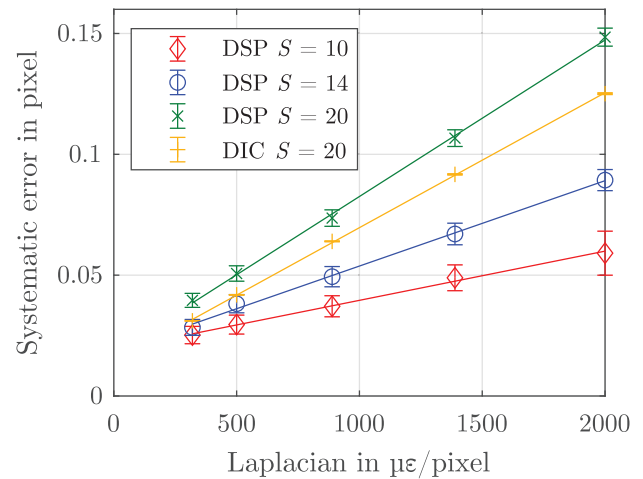


Figure 6. Systematic error over the Laplacian for different subset sizes S . The solid lines are linear fits through the data points and the error bars represent the respective random error. The error values are evaluated from laser speckle patterns (DSP) and evaluated directly from the deformed surface topography (DIC).

leads to a robust result and allows a better calculation of strain fields. However, the associated spatial low-pass filtering also increases the occurrence of systematic errors in the presence of higher-order displacement gradients.

The dependence of the systematic error on the Laplacian and the subset size S is shown in Figure 6. Here, a mean value of the absolute systematic error in sections II and III is plotted over the Laplacian. The solid lines are linear fits through the data points and the error bars represent the respective random error. In the considered interval, the systematic error is linearly dependent on the Laplacian, which is in accordance with the findings of Xu concerning DIC with white light speckle [23] that were discussed in the introduction. The systematic error of the DSP result is around 15% higher than the systematic error of the DIC result. The relatively small deviation of 15% indicates that the systematic error in the presence of higher-order displacement gradients is predominantly caused by the DIC algorithm and only partly by the decorrelation of the laser speckles. Note that the dependence of the systematic error on the subset size is inverse to that of the random error shown in Figure 4. Thus, with respect to the subset size, an optimization problem arises that is subject to the occurring first- and second-order gradients. Additionally, the characteristic of the DIC results is different from the random error. While the random error of the DIC data is negligible, its systematic error is significant and follows the same characteristic as the DSP error.

4.3 Applications

In order to address the third research question concerning DSP in in-process applications, previously published results measured during laser hardening [32], grinding [21] and single-tooth milling [20] are re-evaluated. For a detailed

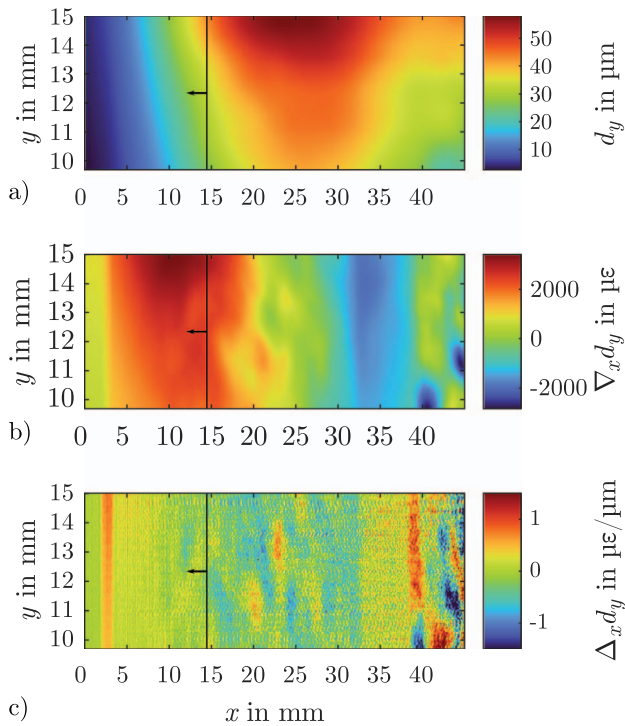


Figure 7. (a) Displacement field d_y measured with DSP during the laser hardening process. The vertical, black line indicates the position of the laser, which is moving in the negative x -direction. (b) First-order gradient $\nabla_x d_y$ of the displacement field. (c) Second-order gradient $\Delta_x d_y$ of the displacement field.

description of each measurement setup and evaluation method, please refer to the original publications.

First, we consider the heat treating process of laser hardening. Since the heat source, i.e., the laser illuminated region is highly localized, high temperature gradients occur on the workpiece surface. Figure 7a shows the resulting displacement field d_y that was measured with DSP and in 7b and 7c the first-order gradient field $\nabla_x d_y$ and the second-order gradient field $\Delta_x d_y$, respectively, are shown. The position of the laser, which moves in the negative x -direction, is indicated by the vertical black line. Due to the heat exposure, an area of high local displacements forms close behind the laser and the area of the highest displacement gradient occurs immediately in front of the laser. Although relatively high local displacements of almost 60 μm occur, they are distributed over a large area of many square millimeters. As a result, the resulting first-order gradients are an order of magnitude lower than the gradient in Figure 4 and the resulting second-order gradients are two orders of magnitude lower than the respective values in Figure 6. Thus, the comparison with the results of the simulative study suggests that random and systematic errors due to displacement gradients are negligible in the considered DSP measurement of the laser hardening process.

Second, the grinding process is considered. Figure 8a shows the displacement field d_y measured with DSP. The region of interest is directly below the grinding wheel during tool engagement. The displacement field reaches up to about 150 μm from the grinding wheel, since sparks and

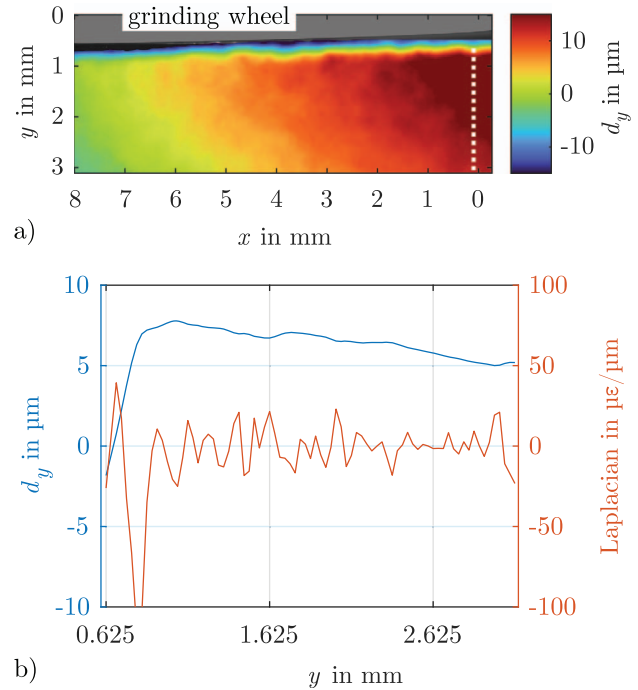


Figure 8. (a) Displacement field d_y measured with DSP during grinding. (b) Local displacements and Laplacian in y -direction. The position of the observed y -interval is indicated by a dotted, white line in (a).

separated chips interfere with the evaluation directly below the grinding wheel. In addition, a burr forms at the edge of the newly machined surface, which leads to out-of-plane displacements and, thus, to speckle decorrelation. Figure 8b shows the local displacements and the Laplacian in a y -interval just behind of the contact zone of tool engagement. The interval is indicated in Figure 8a with a white, dotted line. The displacement first increases abruptly to about 7 μm and then slowly decreases to about 5 μm . Except for an initial extreme value, the gradient remains $< \pm 3000 \mu\epsilon$ and the Laplacian is $\pm 25 \mu\epsilon/\mu\text{m}$. Thus, from the results of the simulative study, we expect random errors in the range of $\pm 4 \times 10^{-3}$ pixels equating to $\pm 120 \text{ nm}$ as well as systematic errors in the range of $\pm 3 \times 10^{-3}$ pixels equating to $\pm 90 \text{ nm}$. However, as the second-order Gradient is determined from a measurement, which contains noise, it does not assume a constant value but fluctuates heavily, errors resulting from the Laplacian are rather random in nature and a valid correction of systematic errors is challenging. Therefore, both sources of error have to be considered in the measurement uncertainty budget of the DSP grinding measurement. The yet unmeasured contact zone in close proximity to the tool is of particular interest for further investigations, as high displacement gradients are expected close to the grinding wheel that likely result in significant random and systematic errors.

Finally, we investigate the process of single-tooth milling. Here, the load is highly concentrated on the cutting edge of the tool. Figure 9a shows the displacement field measured with DSP shortly after tool engagement. Note

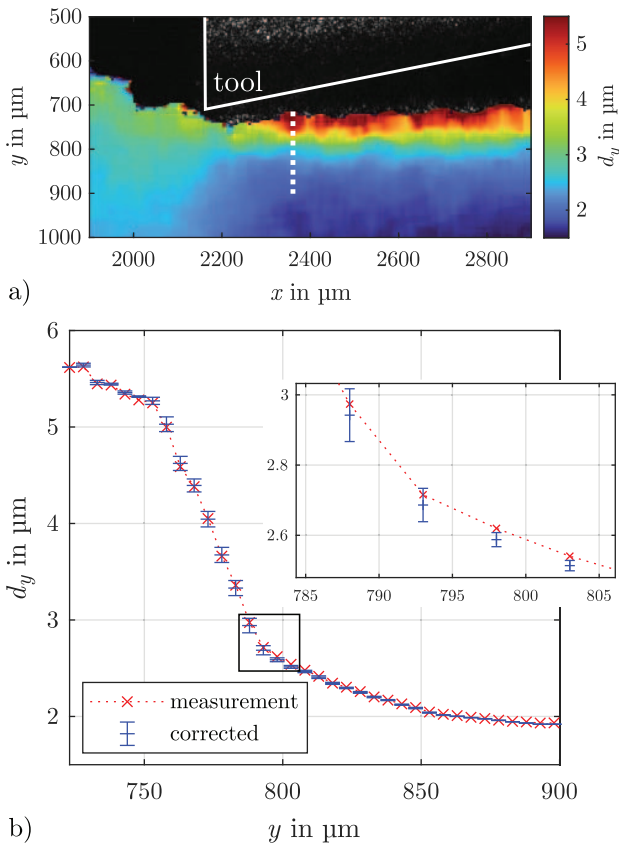


Figure 9. (a) Displacement field d_y measured with DSP during single-tooth milling. (b) Measured local displacements in y -direction and approximate correction of systematic errors. The error bars indicate the random error that is caused by the first-order gradient. The position of the observed y -interval is indicated by a dotted, white line in (a).

the scaling of the axes in micrometers. Whereas in the laser hardening and milling measurements a range of many millimeters were considered, here the field of view is only about 0.3×1 mm. The local displacement in a y -interval just after tool impact is shown in Figure 9b. The y -interval is indicated in (a) with a white, dotted line. The characteristic of d_y with a rapid decrease from a higher level to a lower one is similar to the simulated behavior shown in Figure 5a. The highest first-order displacement gradients of around $7 \times 10^4 \mu\epsilon$ occur from $y = 760 \mu\text{m}$ to $790 \mu\text{m}$. The subset size is 10×10 pixels and, thus, from Figure 4 we interpolate a maximum random error of 0.075 pixels, which equates to 75 nm. The approximate, local random error is indicated with blue error bars. In addition, an approximated correction of the systematic measurement errors is conducted. The Laplacian of d_y assumes maximum values of around $700 \mu\epsilon/\mu\text{m}$ for which we expect systematic errors of 0.033 pixels, which is one order of magnitude larger than the maximum systematic errors approximated for the grinding experiment and equates to 33 nm. Using the fitted model curves from the simulation results shown in Figure 6, the systematic errors of d_y are now estimated and corrected for the measured data. Note that the maximum random and systematic errors occur at different positions. In the

y -interval from $785 \mu\text{m}$ to $805 \mu\text{m}$ that is shown enlarged in Figure 9b first the random error and then the systematic error dominate.

The additional random errors due to camera grayscale resolution, signal-to-noise ratio and light intensity distribution of the speckles are calculated to be 27.5 nm for this experiment using equation (6) of [20]. Thus, random and systematic errors that are induced by displacement gradients locally contribute significantly to the overall measurement uncertainty budget of DSP during milling. However, even in the presence of the high displacement gradients during the milling process, the relative measurement error remains below 2.5% of the respective displacement value. Thus, all three in-process applications that were evaluated are not adversely affected to a significant degree by measurement errors due to displacement gradients. Therefore, the suitability of DSP for laser hardening, grinding and milling is confirmed.

5 Conclusions

We presented a simulation setup for the analysis of random and systematic errors in DSP that are caused by displacement gradients. For that purpose, random surface topographies were generated and deformed with a formalized displacement field that is comprised of sections of constant displacement and of constant second-order displacement gradients. From the original and deformed surface topographies, speckle patterns were simulated and evaluated with a global approach DIC algorithm.

The simulative study has shown that the random error is approximately proportional to the first-order gradient and inversely proportional to the subset size. For first-order gradients smaller than 3% and subsets $\geq 10 \times 10$ pixels, the random errors are below 0.04 pixels and thus smaller than other random error sources, which commonly are >0.05 pixels. The investigations have also shown that the random errors occurring in the presence of displacement gradients are exclusively caused by decorrelation of the laser speckle patterns and not by the DIC algorithm.

The systematic error was found to be linearly dependent on the second-order displacement gradient and the subset size. Thus, the systematic error for DSP in the presence of displacement gradients shows the same characteristics as for DIC with white light speckles. In contrast to the random error, around 85% of the systematic error of DSP is caused by the DIC algorithm and only the small remaining part is attributed to a decorrelation of the laser speckle pattern. For DSP in the presence of displacement gradients, the systematic error is generally in the same range as the random error, e.g., 0.05 pixels for a subset size of 20×20 pixels and a second-order gradient of $500 \mu\epsilon/\mu\text{m}$. Therefore, if high gradients occur, a correction of the systematic errors can significantly reduce the overall measurement uncertainty of DSP.

Finally, we re-evaluated displacement fields measured with DSP during laser hardening, grinding and single-tooth milling. In milling, the highest first-order gradients of $7 \times 10^4 \mu\epsilon$ were measured resulting in a systematic error of 0.075 pixels as well as second-order displacement gradients

of around $700 \mu\epsilon/\mu\text{m}$ resulting in a systematic error of 0.033 pixels. Thus, the measurement errors induced by displacement gradients are locally higher than the cumulative random error due to camera grayscale resolution, signal to noise ratio and light intensity distribution of the speckle patterns. However, since the relative error resulting from displacement gradients is below 2.5% for all three in-process measurements, it can be confirmed that DSP is not adversely affected to a significant degree by displacement gradients in laser hardening, grinding and milling and, thus, is suitable for these in-process applications.

For process optimization in manufacturing applications, a reliable, high-resolution measurement of surface deformation is necessary. As we demonstrated, significant random and systematic deviations can result from deformation gradients, especially in areas subject to high local loads. Therefore, we further plan to perform experiments where deformation gradients occur in a controlled setting. These experiments could enable a validation of the simulative results we have presented in this study. In addition, the experimental results of other manufacturing applications, such as the forming processes rolling, swaging, and sheet metal working, should be investigated for deformation gradients in order to extend the correction of systematic measurement errors to further fields of application. Finally, in order to theoretically evaluate random and systematic errors from a variety of realistic surface deformations, an FEM-simulation could be used in conjunction with our methodology.

Declaration of competing interest

The authors declare that they have no known competing financial interests or personal relationships that could have appeared to influence the work reported in this paper.

Acknowledgments. The authors gratefully acknowledge the financial support for the study design, collection and analysis of the experimental data presented in Section 4.3 by the German Research Foundation (DFG) for subproject C06 “Surface optical measurement of mechanical working material loads” within the Transregional Cooperative Research Center SFB/TRR136. The funding source had no involvement in the decision to publish this article.

Data availability

Data underlying the results presented in this paper are not publicly available at this time but may be obtained from the authors upon reasonable request.

References

- Novovic D., Aspinwall D.K., Dewes R.C., Bowen P., Griffiths B. (2016) The effect of surface and subsurface condition on the fatigue life of Ti-25V-15Cr-2Al-0.2C %wt alloy, *CIRP Ann.* **65**, 1, 523–528.
- Brinksmeier E., Klocke F., Lucca D.A., Sölter J., Meyer D. (2014) Process signatures – a new approach to solve the inverse surface integrity problem in machining processes, *Procedia CIRP* **13**, 429–434.
- Pan B., Qian K., Xie H., Asundi A. (2009) Two-dimensional digital image correlation for in-plane displacement and strain measurement: a review, *Meas. Sci. Technol.* **20**, 6, 062001.
- Berfield T.A., Patel J.K., Shimmin R.G., Braun P.V., Lambros J., Sottos N.R. (2006) Fluorescent image correlation for nanoscale deformation measurements, *Small (Weinheim an der Bergstrasse, Germany)* **2**, 5, 631–635.
- Reagan D., Sabato A., Niezrecki C. (2017) Unmanned aerial vehicle acquisition of three-dimensional digital image correlation measurements for structural health monitoring of bridges, in *Nondestructive Characterization and Monitoring of Advanced Materials, Aerospace, and Civil Infrastructure 2017*. SPIE Proceedings, H.F. Wu, A.L. Gyekenyesi, P.J. Shull, T.-Y. Yu (eds.), SPIE, p. 1016909.
- Yang J., Bhattacharya K. (2019) Augmented Lagrangian digital image correlation, *Exp. Mech.* **59**, 2, 187–205.
- Jin H. (2005) Theoretical development for pointwise digital image correlation, *Opt. Eng.* **44**, 6, 067003.
- Dong Y.L., Pan B. (2017) A review of speckle pattern fabrication and assessment for digital image correlation, *Exp. Mech.* **57**, 8, 1161–1181.
- Goodman J.W. (2007) *Speckle phenomena in optics: Theory and applications*, Roberts, Englewood, CO.
- Fricke-Begemann T. (2003) Three-dimensional deformation field measurement with digital speckle correlation, *Appl. Opt.* **42**, 34, 6783–6796.
- Tausendfreund A., Stöbener D., Fischer A. (2021) In-process measurement of three-dimensional deformations based on speckle photography, *Appl. Sci.* **11**, 11, 4981.
- Larsson L., Sjö Dahl M., Thuvander Fredrik (2004) Microscopic 3-D displacement field measurements using digital speckle photography, *Opt. Lasers Eng.* **41**, 5, 767–777.
- Fu S. (2005) Single-axis combined shearography and digital speckle photography instrument for full surface strain characterization, *Opt. Eng.* **44**, 2, 025602.
- Fischer A. (2017) Fundamental uncertainty limit for speckle displacement measurements, *Appl. Opt.* **56**, 25, 7013–7019.
- Schweickhardt L., Tausendfreund A., Stobener D., Fischer A. (2021) Noise reduction in high-resolution speckle displacement measurements through ensemble averaging, *Appl. Opt.* **60**, 7, 1871–1880.
- Alexe G., Tausendfreund A., Stobener D., Langstadtler L., Herrmann M., Schenck C., Fischer A. (2020) Uncertainty and resolution of speckle photography on micro samples, *Nanomanuf. Metrol.* **3**, 2, 91–104.
- Bender N., Ylmaz H., Bromberg Y., Cao H. (2018) Customizing speckle intensity statistics, *Optica* **5**, 5, 595.
- Viotti M.R., Kaufmann G.H. (2004) Accuracy and sensitivity of a hole drilling and digital speckle pattern interferometry combined technique to measure residual stresses, *Opt. Lasers Eng.* **41**, 2, 297–305.
- Song J.L., Yang J.H., Liu F., Lu K. (2018) High temperature strain measurement method by combining digital image correlation of laser speckle and improved RANSAC smoothing algorithm, *Opt. Lasers Eng.* **111**, 8–18.
- Tausendfreund A., Stöbener D., Fischer A. (2018) Precise in-process strain measurements for the investigation of surface modification mechanisms, *J. Manuf. Mater. Process.* **2**, 1, 9.
- Tausendfreund A., Borchers F., Kohls E., Kuschel S., Stöbener D., Heinzl C., Fischer A. (2018) Investigations

- on material loads during grinding by speckle photography, *J. Manuf. Mater. Process.* **2**, 4, 71.
- 22 Sjödaahl M. (1997) Accuracy in electronic speckle photography, *Appl. Opt.* **36**, 13, 2875–2885.
- 23 Xu X., Su Y., Zhang Q. (2017) Theoretical estimation of systematic errors in local deformation measurements using digital image correlation, *Opt. Lasers Eng.* **88**, 265–279.
- 24 Tong J. (2018) Full-field characterisation of crack tip deformation and fatigue crack growth using digital image correlation—a review, *Fatigue Fract. Eng. Mater. Struct.* **41**, 9, 1855–1869.
- 25 Kirugulige M.S., Tippur H.V. (2009) Measurement of fracture parameters for a mixed-mode crack driven by stress waves using image correlation technique and high-speed digital photography, *Strain* **45**, 2, 108–122.
- 26 Blaber J., Adair B., Antoniou A. (2015) Ncorr: Open-source 2D digital image correlation Matlab software, *Exp. Mech.* **55**, 6, 1105–1122.
- 27 Lu H., Cary P.D. (2000) Deformation measurements by digital image correlation: Implementation of a second-order displacement gradient, *Exp. Mech.* **40**, 4, 393–400.
- 28 Schreier H.W., Sutton M.A. (2002) Systematic errors in digital image correlation due to undermatched subset shape functions, *Exp. Mech.* **42**, 3, 303–310.
- 29 Yu L., Pan B. (2015) The errors in digital image correlation due to overmatched shape functions, *Meas. Sci. Technol.* **26**, 4, 045202.
- 30 Fung A.K., Chen M.F. (1985) Numerical simulation of scattering from simple and composite random surfaces, *J. Opt. Soc. Am. A* **2**, 12, 2274–2284.
- 31 Zhou P., Goodson K. (2001) Subpixel displacement and deformation gradient measurement using digital image/speckle correlation, *Opt. Eng.* **40**, 8, 1613–1620.
- 32 Tausendfreund A., Frerichs F., Stöbener D., Fischer A. (2022) Experimental validation of workpiece deformation simulations by means of rigorous boundary condition analysis, *Procedia CIRP* **108**, 341–345.